Organic Aerosol Formation Downwind from the Deepwater Horizon Oil Spill

J. A. de Gouw, *et al.*

Science **331**, 1295 (2011);
DOI: 10.1126/science.1200320

pre-mRNAs (Fig. 5, B to D, and figs. S14 and S19). As seen with U1, multiple NTC binding events could be detected on the splicing reporter pre-mRNA (4 ± 2% of pre-mRNAs both lost their intron signal and acquired NTC more than once) (fig. S16). The number of binding events observed per pre-mRNA molecule was dependent on the subcomplex being studied. U1 exhibited by far the largest number of binding events, with the number of events systematically decreasing for each successive subcomplex in the pathway (fig. S20). This suggests that at each step of subcomplex addition, some fraction of the pre-mRNA molecules are lost to side pathways that do not lead to productive splicing (Fig. 5E).

Discussion. Taken together, the data from this real-time kinetic analysis of spliceosome assembly are consistent with existing models and lead to new insights. Spliceosome assembly on the RP51A substrate is highly ordered (U1 → U2 → tri-snRNP → NTC), and pre-association of the subcomplexes is not required for splicing. Although no single step appears to irreversibly commit this pre-mRNA to splicing, commitment increases as spliceosome assembly proceeds. Further, spliceosome assembly on this pre-mRNA is kinetically efficient, with no single subcomplex binding step predominantly restricting the overall rate. Finally, we have directly observed multiple binding events for all subcomplexes, demonstrating that subcomplex binding is reversible. Together, these findings have important implications for the regulation of alternative splicing. If spliceosome assembly is reversible and no single assembly step irreversibly commits a particular pair of splice sites to splicing, then alternative splice site choice can potentially be regulated at any stage of assembly. This hypothesis is bolstered by observations that some regulation of alternative splicing apparently occurs at late stages of assembly (*23*, *24*).

By making possible kinetic analysis of spliceosome assembly in whole-cell extracts, this work opens the door to answering fundamental questions concerning the mechanisms of pre-mRNA splicing. The combination of CoSMoS with chemical and genetic tools is a powerful approach for elucidating the mechanisms of complex biological processes, even when those processes can only be studied in cell extracts. These methods should prove broadly useful for analyzing many other complex macromolecular machines.

References and Notes

1. T. W. Nilsen, *Bioessays* **25**, 1147 (2003).
2. P. Fabrizio *et al.*, *Mol. Cell* **36**, 593 (2009).
3. M. C. Wahl, C. L. Will, R. Lührmann, *Cell* **136**, 701 (2009).
4. S. W. Stevens *et al.*, *Mol. Cell* **9**, 31 (2002).
5. Y. Z. Xu *et al.*, *EMBO J.* **23**, 376 (2004).
6. M. Schneider *et al.*, *Mol. Cell* **38**, 223 (2010).
7. J. Abelson *et al.*, *Nat. Struct. Mol. Biol.* **17**, 504 (2010).
8. C. K. Tseng, S. C. Cheng, *Science* **320**, 1782 (2008).
9. L. Liu, C. C. Query, M. M. Konarska, *Nat. Struct. Mol. Biol.* **14**, 519 (2007).
10. L. J. Friedman, J. Chung, J. Gelles, *Biophys. J.* **91**, 1023 (2006).
11. D. J. Crawford, A. A. Hoskins, L. J. Friedman, J. Gelles, M. J. Moore, *RNA* **14**, 170 (2008).
12. A. Juillerat *et al.*, *Chem. Biol.* **10**, 313 (2003).
13. L. W. Miller, Y. Cai, M. P. Sheetz, V. W. Cornish, *Nat. Methods* **2**, 255 (2005).
14. R. M. Dickson, A. B. Cubitt, R. Y. Tsien, W. E. Moerner, *Nature* **388**, 355 (1997).
15. I. Rasnik, S. A. McKinney, T. Ha, *Nat. Methods* **3**, 891 (2006).
16. S. M. Dunn, R. W. King, *Biochemistry* **19**, 766 (1980).
17. R. Dave, D. S. Terry, J. B. Munro, S. C. Blanchard, *Biophys. J.* **96**, 2371 (2009).
18. B. Séraphin, M. Rosbash, *EMBO J.* **10**, 1209 (1991).
19. R. M. Lardelli, J. X. Thompson, J. R. Yates 3rd, S. W. Stevens, *RNA* **16**, 516 (2010).
20. Materials and methods are available as supporting material on *Science* Online.
21. S. W. Ruby, *J. Biol. Chem.* **272**, 17333 (1997).
22. P. Legrain, B. Seraphin, M. Rosbash, *Mol. Cell. Biol.* **8**, 3755 (1988).
23. M. Chen, J. L. Manley, *Nat. Rev. Mol. Cell Biol.* **10**, 741 (2009).
24. S. Bonnal *et al.*, *Mol. Cell* **32**, 81 (2008).

25. We thank J. Chung, A. Okonechnikov, J. Yan, J. Haber, S. Lovett, I. Correa, M.-Q. Xu, Z. Chen, and B. Smith for helpful discussions and assistance. This work was supported by NIH RO1s GM043369 (J.G.), GM81648 (J.G.), GM053007 (M.J.M), GM54469 (V.W.C.), RC1 GM091804 (V.W.C), National Research Service Award fellowship GM079971 (A.A.H.), and K99/R00 GM086471 (A.A.H.). D.J.C., S.S.G., and R.W were supported by NIH training grant GM759628, a National Defense Science and Engineering Graduate fellowship, and a Deutscher Akademischer Austausch Dienst fellowship, respectively. M.J.M. is a Howard Hughes Medical Institute investigator. V.W.C. holds patents on the TMP-tag technology, and the technology is licensed and commercialized by Active Motif.

Supporting Online Information

www.sciencemag.org/cgi/content/full/331/6022/1289/DC1
Materials and Methods
Figs. S1 to S21
Scheme S1
Tables S1 to S12
Movies S1 to S3
References

7 October 2010; accepted 28 January 2011
10.1126/science.1198830

Organic Aerosol Formation Downwind from the Deepwater Horizon Oil Spill

J. A. de Gouw,[1,2]* A. M. Middlebrook,[1] C. Warneke,[1,2] R. Ahmadov,[1,2] E. L. Atlas,[3] R. Bahreini,[1,2] D. R. Blake,[4] C. A. Brock,[1] J. Brioude,[1,2] D. W. Fahey,[1] F. C. Fehsenfeld,[1,2] J. S. Holloway,[1,2] M. Le Henaff,[3] R. A. Lueb,[5] S. A. McKeen,[1,2] J. F. Meagher,[1] D. M. Murphy,[1] C. Paris,[3] D. D. Parrish,[1] A. E. Perring,[1,2] I. B. Pollack,[1,2] A. R. Ravishankara,[1] A. L. Robinson,[6] T. B. Ryerson,[1] J. P. Schwarz,[1,2] J. R. Spackman,[1,2] A. Srinivasan,[3] L. A. Watts[1,2]

A large fraction of atmospheric aerosols are derived from organic compounds with various volatilities. A National Oceanic and Atmospheric Administration (NOAA) WP-3D research aircraft made airborne measurements of the gaseous and aerosol composition of air over the Deepwater Horizon (DWH) oil spill in the Gulf of Mexico that occurred from April to August 2010. A narrow plume of hydrocarbons was observed downwind of DWH that is attributed to the evaporation of fresh oil on the sea surface. A much wider plume with high concentrations of organic aerosol (>25 micrograms per cubic meter) was attributed to the formation of secondary organic aerosol (SOA) from unmeasured, less volatile hydrocarbons that were emitted from a wider area around DWH. These observations provide direct and compelling evidence for the importance of formation of SOA from less volatile hydrocarbons.

On 20 April 2010, the Deepwater Horizon (DWH) offshore drilling unit exploded, causing the riser pipe to rupture and crude oil to flow into the Gulf of Mexico from a depth of ~1500 m. The oil leak rate was estimated to be 68,000 barrels per day (*1*), and much of that oil accumulated on the sea surface. A NOAA WP-3D research aircraft equipped with a large number of instruments to characterize trace gases and aerosols (*2*) performed two flights near DWH on 8 and 10 June to explore the atmospheric impacts of the spilled oil and of the cleanup activities near DWH. This report discusses one of those impacts: the formation of large concentrations of secondary organic aerosol (SOA) observed downwind from the oil spill. These findings have implications for our general understanding of organic aerosol, which is a large but poorly understood class of atmospheric aerosol

[1]Chemical Sciences Division, Earth System Research Laboratory, National Oceanic and Atmospheric Administration, Boulder, CO 80305, USA. [2]Cooperative Institute for Research in Environmental Sciences, University of Colorado, Boulder, CO 80309, USA. [3]Rosenstiel School of Marine and Atmospheric Science, University of Miami, Miami, FL 33149, USA. [4]Department of Chemistry, University of California, Irvine, CA 92697, USA. [5]Atmospheric Chemistry Division, Earth System Laboratory, National Center for Atmospheric Research, Boulder, CO 80301, USA. [6]Center for Atmospheric Particle Studies, Carnegie Mellon University, Pittsburgh, PA 15213, USA.

*To whom correspondence should be addressed. E-mail: joost.degouw@noaa.gov

that affects air quality and climate change (*3*). A parallel analysis of data from the flights over the oil spill focused on the quantification of atmospheric emissions in general, on the air-water partitioning of volatile organic compounds (VOCs), and on an estimate of the oil leak rate (*4*).

A large fraction of aerosol in the atmosphere consists of organic material (*5*). In the polluted atmosphere, the dominant fraction of this organic aerosol (OA) is secondary (*6*): It is formed in the atmosphere from gas-phase species. Recent research has indicated that SOA formation in polluted air is much more efficient than expected from the measured VOCs [volatile is defined here as having an effective saturation concentration, C*, of $>10^6$ μg m^{-3} (*7*)] and from their particulate mass yields as determined in the laboratory (*8*–*11*). One potential explanation for this discrepancy is the formation of SOA from semivolatile organic compounds (SVOCs; C* = 10^{-1} to 10^3 μg m^{-3}) or organic compounds of intermediate volatility (IVOCs; C* = 10^3 to 10^6 μg m^{-3}) (*7*, *12*). Because SVOCs and IVOCs are typically co-emitted with VOCs, this mechanism has not been unambiguously observed in the atmosphere. As a result, it is currently unknown how much of the discrepancy between measured and expected SOA can be attributed to formation from SVOCs and IVOCs. The oil spill provided a unique environment to study SOA formation from VOCs and IVOCs separately, because organic compounds were released from different parts of the oil slick depending on their volatility.

During both flights over the oil slick, a narrow plume of VOCs and a much wider plume of OA were observed downwind of DWH (Fig. 1). Results from the 10 June 2010 flight are discussed here in detail, as higher and more constant wind speeds on this day led to a more easily interpretable data set. The extent of the surface oil slick on 10 June (Fig. 1) is estimated from a composite of multiple satellite instruments (*13*). VOCs and OA were not enhanced everywhere over the oil but were instead confined to much narrower plumes downwind of DWH. Data from two periods (defined in Fig. 1C) are further examined in Fig. 2. Period P1 represents the measurements made closest to DWH; period P2 was farthest from DWH.

The evaporation of freshly surfaced oil was the dominant source of the VOCs measured downwind of DWH (*4*). In laboratory analyses of oil spilled at DWH (*14*), the first 23% of the mass evaporated within 2 hours (fig. S1). During a 2-hour period, the sea surface transport of oil is a few kilometers at most, which explains why the VOCs were emitted from only a small area and confined to a narrow plume (Fig. 1C). As described elsewhere in detail (*4*), the composition of VOCs measured in canister samples collected in the plumes was dominated by alkanes and aromatics. The relative abundance of the VOCs measured in the atmosphere reflected the composition of the spilled oil itself, with the exception of a subset of lighter VOCs that dissolved either completely or partially during transport from the sea bottom to the surface. Other sources of VOCs (e.g., from ships and flares) were much smaller and had a different VOC composition; burning of surface oil did not occur on 10 June.

A plume of OA was observed downwind of DWH (Fig. 1B), with mass loadings peaking at >25 μg m^{-3} on 8 June and >10 μg m^{-3} on 10 June; these values are in the range of OA observed in U.S. urban atmospheres (*5*). Because the measured OA was not correlated with tracers of incomplete combustion, such as black carbon aerosol and carbon monoxide (Fig. 2), we can rule out a combustion-related source. For reasons outlined below, we argue that the OA was largely formed from vapors released from the oil and the condensation of their atmospheric oxidation products onto existing particles. First, the mass flux of OA increased with distance downwind of DWH. Second, measured particle number size distributions indicated a growth in particle size downwind of DWH (Fig. 2B). This rules out wave-generated emission of aerosol from the sea surface—a known source of aerosol in marine air (*15*)—as the dominant source of OA in this case, because it would have led to the same particle sizes at all downwind distances. Total particle number concentrations, not shown here, remained relatively constant between periods P1 and P2, which, together with the observed increase in aerosol mass (Fig. 2A), rules out coagulation as the primary cause of the growth in particle size.

One further observation regarding the OA is noted here but not explored in detail. Mass spectral analysis of the aerosol (*5*) indicates that both oxygenated organic aerosol (OOA) and hydrocarbon-like organic aerosol (HOA) increased in the aerosol downwind, with a larger contribution from HOA than from OOA (Fig. 2A). Although HOA and OOA are typically

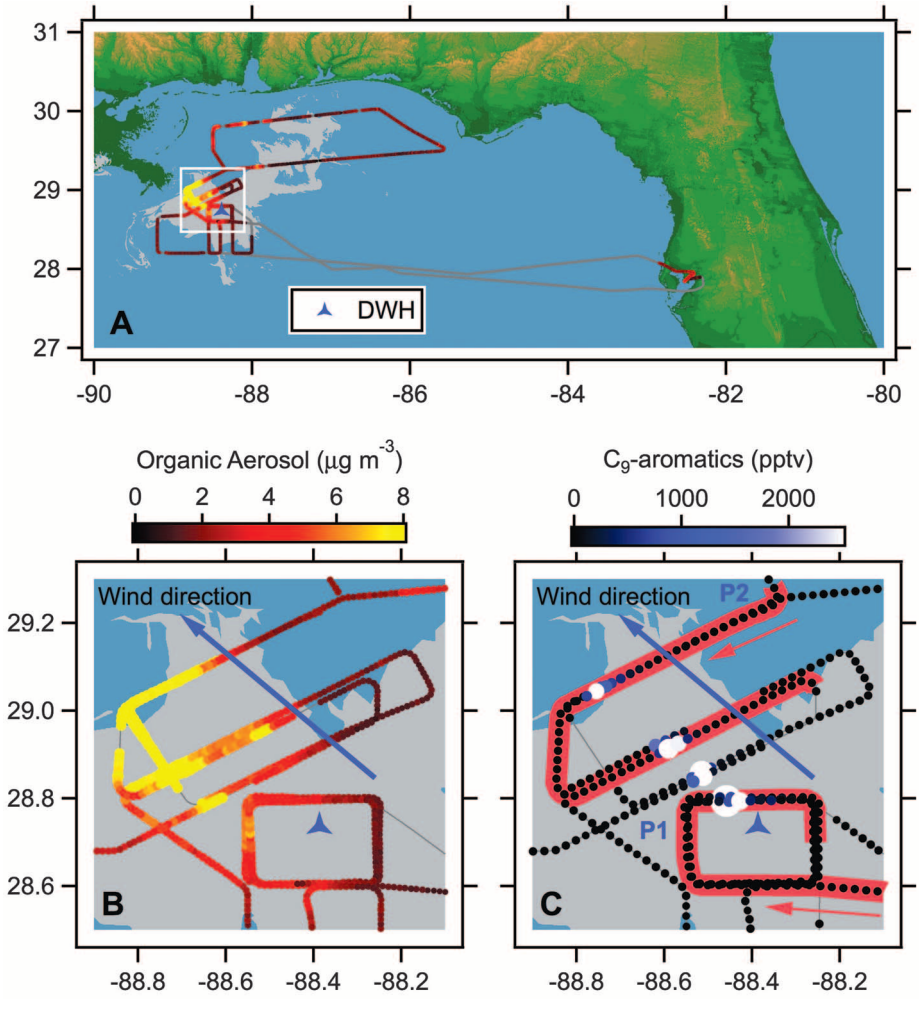

Fig. 1. (**A**) Flight track on 10 June 2010, with data points below 900 m color- and size-coded by the measured concentration of organic aerosol. The gray area underlying the flight track represents the extent of the oil slick derived from multiple satellite observations. (**B** and **C**) The area indicated by the white square in (A) is shown in more detail in (B) and color- and size-coded by the measured C_9-aromatics in (C). Data from the periods P1 and P2, indicated in red in (C) with arrows indicating the flight direction, are shown in more detail in Fig. 2. Degrees latitude and longitude are indicated along the *y* and *x* axes, respectively.

attributed to direct emission from combustion sources and to secondary formation, respectively, our results show that HOA can also be formed in the atmosphere.

Aromatics and C_8 to C_{11} alkanes are known to be SOA precursors (*16*, *17*) and were measured at very high mixing ratios downwind of DWH (Fig. 1C), higher than typically observed in urban areas (*18*, *19*). However, the SOA was not primarily formed from these VOCs, because the observed OA plume was much wider than the VOC plume and because VOCs were not enhanced upwind from the OA plume. Instead, we argue here that IVOCs evaporating from the oil were the SOA precursors. As their evaporation is slower, these species were transported on the sea surface away from the area where the spilled oil surfaced and were released to the atmosphere from a wider area (Fig. 3A). Further evidence for this conceptual model is obtained from the plume widths of the measured VOCs, whose vapor pressures span about two orders of magnitude. Figure 3B shows that close to DWH, the width of the VOC plume increased with the molecular weight of the VOC.

SOA was not additionally enhanced in the narrow VOC plume despite very high mixing ratios of precursors. Calculations with the Weather Research and Forecasting model coupled with Chemistry (WRF-Chem) indicates that the very high VOC mixing ratios combined with moderately enhanced NO_x (1 to 5 parts per billion by volume) resulted in low concentrations of hydroxyl radicals in the narrow VOC plume. Therefore, only a small fraction of the measured VOCs reacted to form SOA in the downwind distance sampled by the aircraft.

What were the precursors of the SOA formed downwind of DWH? We constructed a volatility distribution of the oil (Fig. 4A)—that is, the mass fraction as a function of the effective saturation concentration C* (*7*)—using the hydrocarbon composition of the spilled oil (*4*) and assuming that the value of C* for a hydrocarbon is the same as that for an *n*-alkane with the same number of carbon atoms (fig. S2). Assuming that the evaporation rate of a compound is proportional to its vapor pressure, we can fit the measured evaporation curve for the spilled oil (fig. S1) using the volatility distribution (Fig. 4A) and one free parameter, A, that equates the evaporation rate of each volatility class to $A \times C^*$. The best fit, shown by the envelope of contributions from all volatility classes in Fig. 4B, suggests that for $C^* \geq 10^8$ μg m^{-3} ($\leq C_8$ hydrocarbons), evaporation takes <1 hour. For $C^* = 10^4$ to 10^7 μg m^{-3} (C_9 to C_{18} hydrocarbons), evaporation takes place on time scales varying from 1 to 1000 hours. For $C^* \leq 10^3$ μg m^{-3} ($\geq C_{19}$ hydrocarbons), evaporation takes >1000 hours.

To relate the time scales for evaporation of the precursor VOCs to spatial scales, we used an offline Lagrangian particle transport model to simulate surface oil trajectories on the basis of hourly seawater velocity data from the Naval Research Laboratory's HYCOM-based 0.04° Gulf of Mexico Ocean Prediction system (*20*, *21*). In the model, 1000 to 5000 particles representing freshly surfaced oil were released within an area of 4 km by 4 km, and their spreading on the sea surface due to advection, wind drift, and parameterized subgrid scale diffusion was described. From the time since surfacing, the model calculates the area where emissions to the atmosphere occur for species with evaporation lifetimes of 1 to 1000 hours, respectively (Fig. 4C and fig. S3). In the model, compounds that evaporate in <10 hours are released to the atmosphere from a small area near DWH, whereas compounds that evaporate in >100 hours are released from an area that is much larger than the extent of the OA plume. We conclude that the compounds responsible for SOA formation were most likely released on evaporation time scales of 10 to 100 hours. The best fit to the evaporation curve in Fig. 4B suggests that on these time scales, evaporation is dominated by $C^* = 10^5$ μg m^{-3} compounds (C_{14} to C_{16} hydrocarbons), and we conclude that these species were the most likely precursors of the observed SOA. The effective saturation concentration (C*) equals the ambient mass loading at which partitioning of a compound shifts between the gas and condensed phases; a C* value of 10^5 μg m^{-3} is much higher than ambient mass loading (~10 μg m^{-3}),

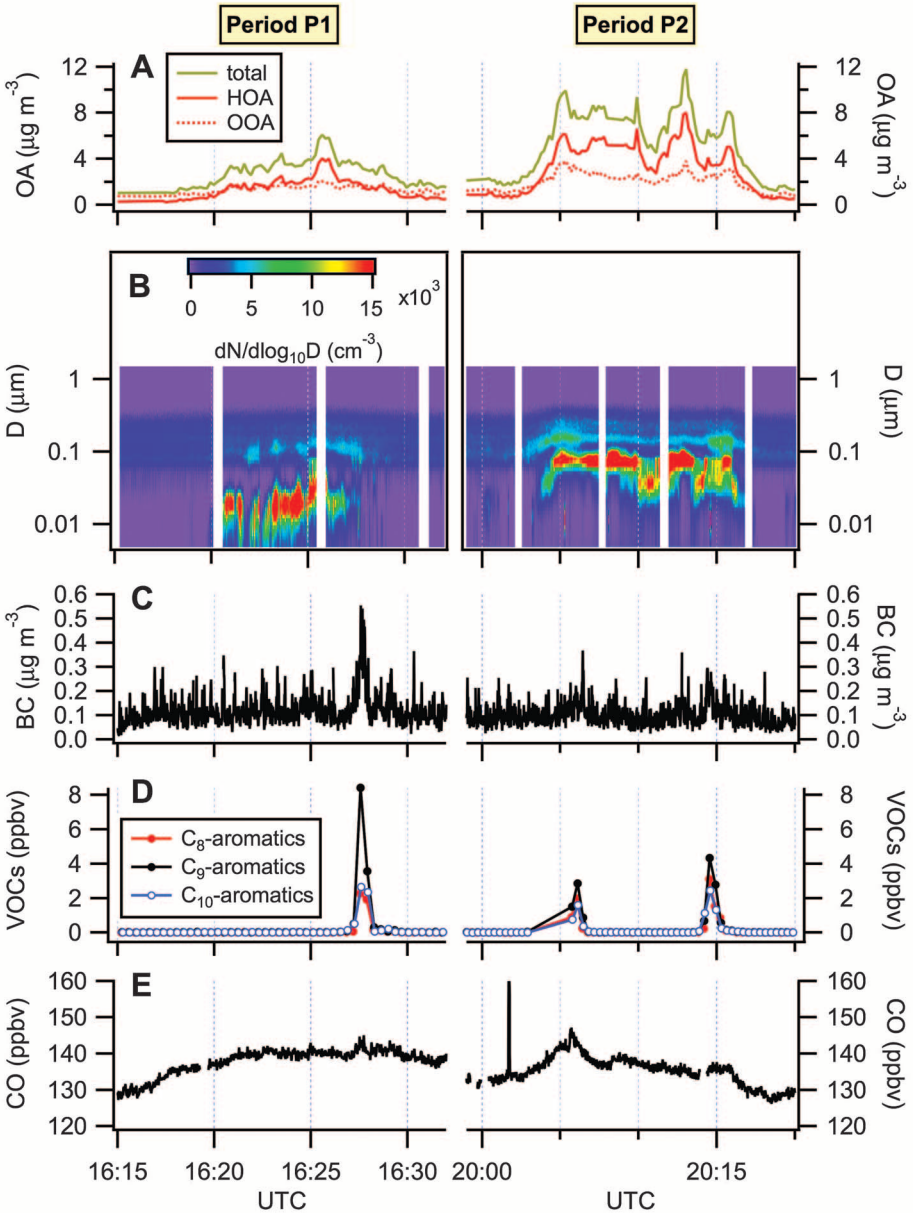

Fig. 2. Time series of selected data from periods P1 and P2 (Fig. 1): (**A**) organic aerosol and its contributions from hydrocarbon-like organic aerosol (HOA) and oxygenated organic aerosol (OOA), (**B**) particle number size distributions, (**C**) black carbon (BC) aerosol, (**D**) aromatic volatile organic compounds (VOCs), and (**E**) carbon monoxide (CO).

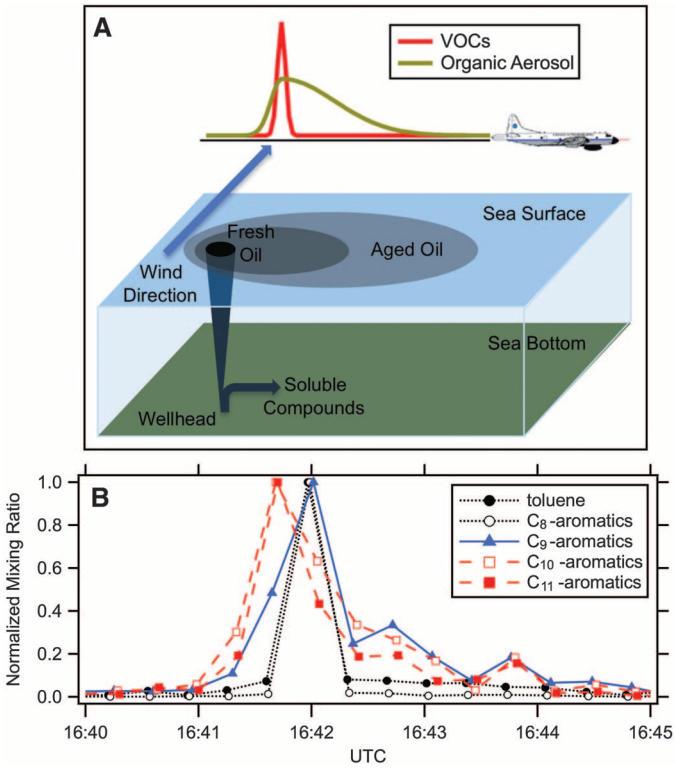

Fig. 3. (**A**) Conceptual model describing the observations of VOCs and organic aerosol downwind from the oil spill. Oil from the leaking riser pipe surfaces in a relatively small area. The most volatile fraction of the oil evaporates within hours, leading to a narrow atmospheric plume of VOCs downwind from the spill site. The less volatile fraction takes longer to evaporate, during which time the oil spreads over a larger area. Organic aerosol is formed from the less volatile fraction and is observed in a wider plume downwind. (**B**) Measurements of different aromatic species shortly downwind from the oil spill demonstrate that the plume broadens as a function of decreasing volatility, in accordance with the conceptual model. Mixing ratios were normalized to their maximum value during this transect to facilitate the comparison of plume shapes.

which suggests that a substantial chemical transformation of these hydrocarbon precursors must take place to lower their volatility and produce SOA. On the basis of the distance of the downwind transect P2 (Fig. 1C) to the DWH spill site (45 km) and the average wind speed (5 m s^{-1}), we estimate that this chemical transformation occurred in <3 hours.

How efficient was SOA formation from C* = 10^5 μg m^{-3} compounds over the oil? The total leak rate of oil from DWH on 10 June was estimated to be 2.03 × 10^6 kg day^{-1} (*4*). Of this total, 11% (2.2 × 10^5 kg day^{-1}) is estimated to be in the C* = 10^5 μg m^{-3} class (Fig. 4A). The flux of OA farthest downwind of DWH (estimated from the integral of the measured concentration times orthogonal wind speed and multiplied by the depth of the boundary layer) (*4*, *22*) was 8 × 10^4 kg day^{-1}, which may be a lower estimate because the aircraft did not sample across the full width of the SOA plume (Fig. 1B). From these numbers, we estimate the SOA yield for C* = 10^5 μg m^{-3} compounds to be ~36%, in approximate agreement with laboratory studies (*12*).

Previous work has suggested that SOA formation from SVOCs and IVOCs could be an important source of aerosol in the United States (*12*). However, field verification of this chemistry has been difficult because SVOCs and IVOCs are typically co-emitted with VOCs; for that

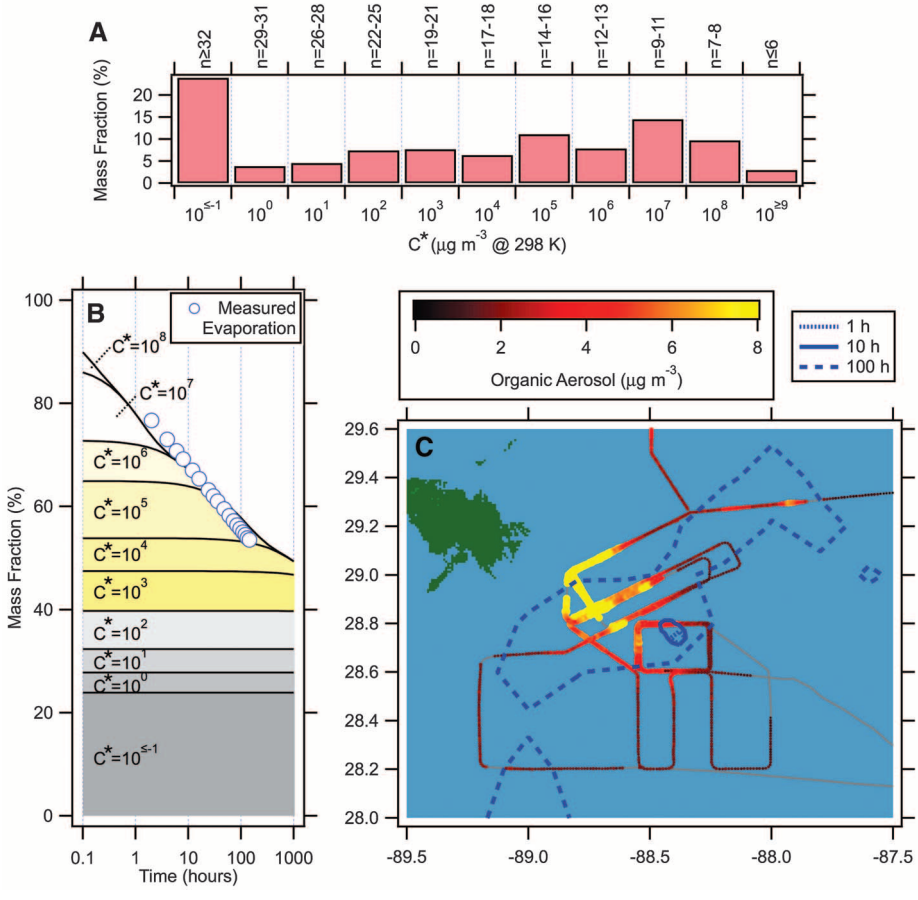

Fig. 4. (**A**) Volatility distribution of oil spilled at DWH derived from the oil composition. The numbers on the top axis indicate the number of carbon atoms of the corresponding hydrocarbons. (**B**) Evaporation of oil as a function of time (blue circles) (*14*) fit using the volatility distribution from (A). (**C**) Modeled distribution of a compound that surfaces at the DWH spill site and evaporates with a mean lifetime of 1, 10, and 100 hours, respectively. The blue curves outline the areas where concentrations are ≥10% of the maximum value. The flight track on 10 June 2010, color-coded by the measured concentration of organic aerosol, is added for comparison.

reason, the SOA observed in polluted air cannot be unambiguously attributed to formation from SVOCs and IVOCs. The DWH oil spill provided a unique look at this chemistry because the emissions of VOCs, IVOCs, and SVOCs were spatially separated and the importance of SOA formation from IVOCs could be clearly demonstrated. These results form a well-constrained case to improve our quantitative understanding of IVOC chemistry, which will help to describe the importance of IVOCs for SOA formation in other polluted regions of the atmosphere.

References and Notes

1. T. J. Crone, M. Tolstoy, *Science* **330**, 634 (2010); 10.1126/science.1195840.
2. See supporting material on *Science* Online.
3. M. Kanakidou *et al.*, *Atmos. Chem. Phys.* **5**, 1053 (2005).
4. T. B. Ryerson *et al.*, *Geophys. Res. Lett.* 10.1029/2011GL046726 (2011).
5. Q. Zhang *et al.*, *Geophys. Res. Lett.* **34**, L13801 (2007).
6. J. de Gouw, J. L. Jimenez, *Environ. Sci. Technol.* **43**, 7614 (2009).
7. A. L. Robinson *et al.*, *Science* **315**, 1259 (2007).
8. J. A. de Gouw *et al.*, *J. Geophys. Res.* **110**, D16305 (2005).
9. R. Volkamer *et al.*, *Geophys. Res. Lett.* **33**, L17811 (2006).
10. H. Matsui *et al.*, *J. Geophys. Res.* **114**, D04201 (2009).
11. D. Johnson *et al.*, *Atmos. Chem. Phys.* **6**, 403 (2006).
12. N. M. Donahue, A. L. Robinson, S. N. Pandis, *Atmos. Environ.* **43**, 94 (2009).
13. NOAA-NESDIS, Satellite Derived Surface Oil Analysis Products—Deepwater Horizon (www.ssd.noaa.gov/PS/MPS/deepwater.html).
14. Spill Related Properties of MC 252 Crude Oil Sample ENT-052210-178, SL Ross Environmental Research Ltd. for British Petroleum (July 2010); see www.restorethegulf.gov/sites/default/files/documents/pdf/OilBudgetCalc_Full_HQ-Print_111110.pdf, Appendix 8.
15. D. V. Spracklen, S. R. Arnold, J. Sciare, K. S. Carslaw, C. Pio, *Geophys. Res. Lett.* **35**, L12811 (2008).
16. N. L. Ng *et al.*, *Atmos. Chem. Phys.* **7**, 3909 (2007).
17. C. E. Jordan *et al.*, *Atmos. Environ.* **42**, 8015 (2008).
18. A. K. Baker *et al.*, *Atmos. Environ.* **42**, 170 (2008).
19. C. Warneke *et al.*, *J. Geophys. Res.* **112**, D10S47 (2007).
20. F. Counillon, L. Bertino, *Ocean Dyn.* **59**, 83 (2009).
21. E. P. Chassignet *et al.*, *Oceanography* **22**, 64 (2009).
22. W. H. White *et al.*, *Science* **194**, 187 (1976).

23. We thank the flight crew of the NOAA WP-3D, as well as NOAA's National Environmental Satellite, Data, and Information Service, for the oil spill maps in Fig. 1. Supported by the NASA Radiation Sciences Program (D.W.F., A.E.P., J.P.S., J.R.S., and L.A.W.), NSF grant 1048697 (C.P., M.L.H., and A.S.) and a U.S. Coast Guard Pollution Removal Funding Authorization to NOAA for flights over the oil spill made by the NOAA WP-3D.

Supporting Online Material

www.sciencemag.org/cgi/content/full/331/6022/1295/DC1
Materials and Methods
Figs. S1 to S3
References

11 November 2010; accepted 3 February 2011
10.1126/science.1200320

Catastrophic Drought in the Afro-Asian Monsoon Region During Heinrich Event 1

J. Curt Stager,[1,2]* David B. Ryves,[3] Brian M. Chase,[4,5] Francesco S. R. Pausata[6,7,8]

Between 15,000 and 18,000 years ago, large amounts of ice and meltwater entered the North Atlantic during Heinrich stadial 1. This caused substantial regional cooling, but major climatic impacts also occurred in the tropics. Here, we demonstrate that the height of this stadial, about 16,000 to 17,000 years ago (Heinrich event 1), coincided with one of the most extreme and widespread megadroughts of the past 50,000 years or more in the Afro-Asian monsoon region, with potentially serious consequences for Paleolithic cultures. Late Quaternary tropical drying commonly is attributed to southward drift of the intertropical convergence zone, but the broad geographic range of the Heinrich event 1 megadrought suggests that severe, systemic weakening of Afro-Asian rainfall systems also occurred, probably in response to sea surface cooling.

Meridional repositioning of the intertropical convergence zone (ITCZ), the primary source of rainfall in most of the tropics, is thought to have been a major source of hydrological variability during the late Quaternary (*1*–*4*). For example, ice sheet expansion forced the mean latitudinal position of the ITCZ southward along with other atmospheric circulation systems in the Northern Hemisphere during the Last Glacial Maximum (*3*), and abrupt North Atlantic cooling during deglacial melting and ice-rafting episodes such as Heinrich stadial 1 (HS-1), along with associated reductions of marine meridional overturning circulation (MOC), is also thought to have had a similar effect on rain belts associated with the ITCZ (*1*, *3*, *4*). Some model simulations of Northern Hemisphere climatic changes associated with HS-1 indicate a southward drift of up to 10 latitudinal degrees (*2*). Most of northern Africa became unusually dry around 16 to 17 thousand calendar years ago (ka) during the HS-1 ice-rafting peak of Heinrich event 1 (H1), including the Sahara and Sahel (*5*), Ethiopia (*6*), and the Red Sea region (*7*), as did most of southern Asia (*8*–*11*) (Figs. 1 and 2). Affecting most of the northern Old World tropics, this arid episode brought some of the most severe drought conditions of the past 50,000 years or more to many of the terrestrial sites that cover such long time periods in detail (Fig. 2 and SOM Text).

Under such circumstances, a more southerly positioned ITCZ would presumably deliver less rain to the northern tropics while causing little change near the equator and wetter conditions in the southern tropics. However, a relative scarcity of high-resolution paleoclimate records from much of the inner and southern tropics has left this commonly cited hypothesis sparsely tested, particularly in Africa. This, in turn, has also limited understanding of the effects of major events such as H1 on global climates. We present a collection of new and recently published records from Africa that register severe aridity in the equatorial and southern tropics about 16 to 17 ka, thereby showing that the H1 megadrought extended far beyond the northern tropics and was therefore one of the most intense and far-reaching dry periods in the history of anatomically modern humans. Together, these records also show that southward drift of the ITCZ cannot have been the only cause of low-latitude drought during H1, and instead suggest that a substantial weakening of tropical rainfall systems also occurred.

If the ITCZ did shift several degrees southward over Africa and Asia during H1, it should still have delivered rains to equatorial regions once or twice annually unless the latitudinal shift was unrealistically large, on the order of 20° or more. However, extreme equatorial drying centered on 16 to 17 ka also occurred in northern Tanzania [(*12*) and this study], Ghana (*13*), and the Niger-Sanaga and Congo watersheds (*14*, *15*) (Fig. 1), as well as in Borneo on the opposite side of the Indian Ocean (*16*), much as it did in the more northerly reaches of the tropics from the Mediterranean Basin to the western Pacific (Figs. 1 to 3 and SOM Text).

A dramatic event associated with these equatorial changes was the desiccation of Lake Victoria, East Africa (Fig. 1), which today is the world's largest tropical lake. With rainfall over the watershed possibly reduced to less than a quarter of its present amount (*7*), the lake dried out twice between 15 and 18 ka, although the timing of the two low stands has previously been unclear (SOM Text). We present here radiocarbon dates and diatom records from two cores, which show that the first of these low stands occurred about 16 to 17 ka (Fig. 3D) (*17*). The disappearance of Lake Victoria would have had severe ecological impacts on regional ecosystems and cultures from

[1]Natural Sciences, Paul Smith's College, Paul Smiths, NY 12970, USA. [2]Climate Change Institute, University of Maine, Orono, ME 04469, USA. [3]Centre for Hydrological and Ecosystem Science, Department of Geography, Loughborough University, Loughborough, LE11 3TU, UK. [4]Institut des Sciences de l'Evolution de Montpellier, UMR 5554 Université Montpellier 2, Bâtiment 22, CC061, Place Eugène Bataillon 34095 Montpellier CEDEX 5, France. [5]Department of Archaeology, History, Cultural Studies and Religion, University of Bergen, 5020 Bergen, Norway. [6]Geophysical Institute, University of Bergen, Allégaten 70, 5007 Bergen, Norway. [7]Bjerknes Centre for Climate Research, Allégaten 55, 5007 Bergen, Norway. [8]European Commission, Joint Research Centre, Institute for Environment and Sustainability, Climate Change Unit, Ispra, Italy.

*To whom correspondence should be addressed. E-mail: cstager@paulsmiths.edu